AC Resistance and Leakage Inductance Estimation for Planar Transformers With Parallel-Connected Windings

Lucas Pniak, Loic Queval, Bertrand Revol, Jean Sylvio Ngoua Teu Magambo, Cyrille Gautier, Olivier Béthoux

▶ **To cite this version:**

Lucas Pniak, Loic Queval, Bertrand Revol, Jean Sylvio Ngoua Teu Magambo, Cyrille Gautier, et al.. AC Resistance and Leakage Inductance Estimation for Planar Transformers With Parallel-Connected Windings. IEEE Transactions on Power Electronics, 2023, 38 (1), pp.728-738. 10.1109/TPEL.2022.3203515 . hal-03835216

HAL Id: hal-03835216
https://hal.science/hal-03835216v1

Submitted on 31 Oct 2022

HAL is a multi-disciplinary open access archive for the deposit and dissemination of scientific research documents, whether they are published or not. The documents may come from teaching and research institutions in France or abroad, or from public or private research centers.

L'archive ouverte pluridisciplinaire **HAL**, est destinée au dépôt et à la diffusion de documents scientifiques de niveau recherche, publiés ou non, émanant des établissements d'enseignement et de recherche français ou étrangers, des laboratoires publics ou privés.

IEEE TRANSACTIONS ON
POWER ELECTRONICS

Publish Manuscript

AC Resistance and Leakage Inductance Estimation for Planar transformers With Parallel-Connected Windings,

Lucas Pniak, Loïc Quéval, Bertrand Revol, Jean-Sylvio Ngoua Teu, Cyrille Gautier and Olivier Béthoux

DOI: 10.1109/TPEL.2022.3203515.

Reference: IEEE-TPEL 2022, Vol. 38, N°. 1, January 2023

Publisher: IEEE

To appear in: ***Transactions on Power Electronics***

Received date: 21 February 2022

Revised date: 30 May 2022 And 2 August 2022

Accepted date: 27 August 2022

Date of Publication: 1 September 2022 (online)

Please cite this article as: L. Pniak, L. Quéval, B. Revol, J. -S. N. Teu, C. Gautier and O. Béthoux, "AC Resistance and Leakage Inductance Estimation for Planar Transformers With Parallel-Connected Windings," in IEEE Transactions on Power Electronics, vol. 38, no. 1, pp. 728-738, Jan. 2023, doi: 10.1109/TPEL.2022.3203515, https://doi.org/ 10.1109/TPEL.2022.3203515.

Document Version: Early version, also known as pre-print

AC resistance and leakage inductance estimation for planar transformers with parallel connected windings

Lucas Pniak[1,2], Loïc Quéval[2], Bertrand Revol[1], Jean-Sylvio Ngoua Teu[1], Cyrille Gautier[1] and Olivier Béthoux[2]

***Abstract*— Regarding the ever-increasing switching frequency of power converters, there is a lack of tools to perform a quick and effective optimization of the high frequency transformers embedded in isolated power converters. Indeed, at high operating frequency, the geometry of the core and windings deeply impacts the overall transformer performance. Specifically, assessing accurately the current distribution in parallel connected windings is a challenging and key issue. Winding parallelization, frequently implemented in low voltage and high current applications so as to decrease Joule losses, may be an ineffective solution because of skin and proximity effects. They create an unbalanced current distribution in the parallel connected windings, which greatly impacts the AC resistance and leakage inductance of the transformer. The present article proposes an innovative frequency analytical model permitting to simply and accurately compute the current distribution in the transformer windings, the AC resistance, and the leakage inductance. The proposed approach is comprehensively presented, validated using both measurements and 2D finite element analysis and analyzed giving guidelines to engineers designing high frequency transformers.**

NOMENCLATURE

α	Wave number.
Δ	Relative skin depth, e/δ.
δ	Skin depth at the fundamental frequency.
$\mathbf{E}$	Electric field (RMS).
$\mathbf{H}$, H	Magnetic field (RMS).
$\mathbf{j}$	Current density (RMS).
$\dot{\mathrm{Q}}$, $\dot{Q}$	Current (RMS).
L_μ	Magnetizing inductance matrix.
L_{lk}	Leakage inductance matrix.
R	Resistance matrix.
μ_0	Permeability of free space, $4\pi \times 10^{-7}$ H/m.
μ_r	Relative permeability of the core material.
ω	Angular frequency.
σ	Conductivity of the conductors material.
d_m	Mean length of a field line in the magnetic core.
e	Thickness of a conductor layers.
e_0	Air gap.
E_μ	Magnetizing energy.
E_{lk}	Leakage magnetic energy.
ei_k	Thickness of the k^{th} insulation layer.
h_c	Width of a conductor layers.
j	$(-1)^{1/2}$.
L_c	Mean length of conductor layers.
L_{AC}	AC leakage inductance.
N	Number of conductor layers.
P_J	Joule losses.
R_{AC}	AC resistance.
S_f	Effective flux area of the core.

[1] Electrical Systems & Electronics Department, SafranTech, SAFRAN, Magny les Hameaux, France

[2] Group of Electrical Engineering - Paris (GeePs), University of Paris-Saclay, CentraleSupélec, CNRS 91192 Gif-sur-Yvette, France & Sorbonne University, CNRS, 75252 Paris, France

I. INTRODUCTION

Like the automotive sector, the aeronautics sector and in particular the equipment manufacturers are currently undergoing profound changes to achieve carbon neutrality in aviation by 2050. These developments concern, among many other aspects, the on-board electrical systems for which the aim is to improve efficiency and reduce weight, while ensuring greater flexibility. The network architectures envisaged for the turbomachines hybridization and continuous on-board generation (270 V, 540 V, etc.) must ensure interconnections with key conventional networks (i.e. 28 V). Isolated modular DC / DC converters (DAB, LLC, etc.) are currently being studied to achieve these interconnections [1]. Using fast components (e.g. GaN) in these topologies enables to reach attractive power densities (> 2 kW/kg) [2]. In these isolated power structures, designing the high-frequency transformer (100 kHz to 1 MHz) may be a challenging issue.

Thanks to their low profile, good thermal characteristics, high manufacturing repeatability and accuracy and possibly predictable parasitic elements [3], [4], [5], [6], [7], planar transformers (Fig. 1) meet the demanding expectations of modern power electronics, specifically regarding switching frequency and power density [8], [9]. In many applications, the high power and low voltage requirements imply using parallel connected windings in order to limit the AC copper losses and enhance the transformer thermal behavior.

Fig. 1: A planar high frequency power transformer.

At high frequencies, the skin and proximity effects increase Joule losses, and also may unbalance the current distribution in parallel connected windings. This imbalance can either have a negative or positive impact on the AC Joule losses depending on the considered operating frequency and winding geometry. In both cases, it significantly impacts the transformer performance. The designer has to accurately assess this current sharing in order to find the optimal transformer design and determine the two main macroscopic transformer parameters, i.e. AC resistance and leakage inductance.

Many methods have been used to solve this electromagnetic problem. 2D or 3D Finite Element Analysis (FEA) simulations [10], [11], [12], [13], [14] provide a very accurate estimation of the magnetic field and current distribution, at the cost of a substantial computation time. Enabling a reduced computation time, analytical methods based on lumped circuit models such as Modular Layer Model (MLM) [15], transmission lines in 1D [16], [17] or 2D [18] also show precise results on a wide frequency band. Implementing these techniques requires a SPICE solver and a software tool to generate SPICE netlist. Finally, a 1D analytical model [19] based on Dowell's hypothesis [20] uses the Maxwell-Faraday theorem on well-chosen closed paths to determine the winding turns electromotive forces as intermediate variables, then deduce the current distribution and ultimately infer AC resistance and leakage inductance as macroscopic energetic parameters. The intermediate calculations make the resolution complex and give no insight in the understanding of the energy phenomena to be optimized.

The present paper proposes an innovative analytical 1D frequency-domain electromagnetic model for planar transformers that may have windings connected in parallel. Based on an energetic approach of system dynamics (Euler-Lagrange), this model directly uses the well-known expressions of the AC Joule losses [21] and leakage magnetic energy [22], [23] to build the linear system governing the current distribution. It avoids to solve the Maxwell-Faraday equations and the associated integral calculation proposed by Wei Chen [19] and does not require a software tool to generate SPICE netlist [15]. The suggested method can be implemented in an automatic tool and enables the accurate computation of the AC resistance and leakage inductance of any winding configuration in a short computation time.

The paper is organized as follows. Section II describes the electromagnetic problem and recalls the Joule power losses and magnetic energies calculation. Section III introduces the procedure for applying Euler-Lagrange equations to the transformer. Computing the energy and power loss functions permits to derive the linear system governing the current distribution, which is the main contribution of the paper. Finally, section IV compares Finite Element Analysis (FEA) simulations and experimental results with the proposed method results in order to validate the suggested approach. Using the energetic approach, the studied examples are fully analyzed and discussed to provide a clear insight into the physics at stake in the transformer.

II. Energy Analysis of the Transformer

A. Definition of the electromagnetic problem

As shown in Fig. 2, a planar transformer composed of N conductor layers and a magnetic core is considered. An index k, $k \in [1, N]$, and a domain Ω_k are assigned to each conductor layer. Ω_k corresponds to the cross section in the (x,z) plane. The currents $\dot{Q}_k$ flow through them generating a magnetic field $\mathbf{H}$ in the winding window. The very specific geometry of the planar transformer enables the following hypothesis:

i) The core permeability is very high. The magnetic field strength inside the core is negligible compared to the leakage magnetic field in the winding window.
ii) The air gap is small enough or far enough from the conductor layers. The fringing effect is neglected.
iii) The conductor width is much greater than its thickness or than the one of the insulation layers. Thus, end effect is neglected and the magnetic field is assumed parallel to the conductor layers. Additionally, an invariance along the z-axis is assumed in the conductor layers.
iv) The model is 2D. An invariance along the y-axis is assumed. The effect of coil heads is neglected.
v) The conductor layers, the insulation layers and the magnetic material are considered linear, homogeneous and isotropic. Core losses are neglected since only short-circuit tests are considered in this paper.
vi) The problem is studied in a harmonic way and in steady state.
vii) The problem is Magneto-Quasi-Static (MQS) [24].

B. Magnetic field distribution in the winding window

1) In the insulation layers: Considering hypothesis i), Ampère theorem applied to the closed paths Γ_k, $k \in [1, N+1]$, defined on Fig. 2, shows that the magnetic field $\mathbf{H}$

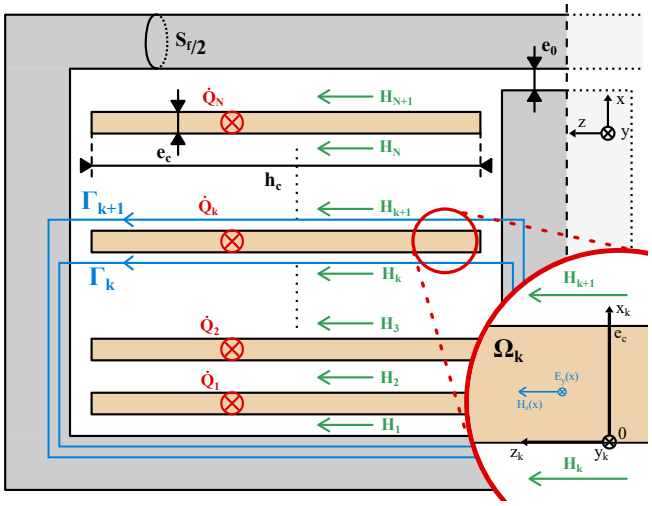

Fig. 2: Definition of the geometric parameters, the currents, the magnetic field in the insulation layers, and of the local coordinate system for each conductor layer Ω_k, $k \in [1, N]$. The dashed line is the symmetry plane.

is uniform in each insulation layers. For each insulation layer k, the magnitude of this field is denoted H_k. The equations resulting from Ampère's theorem highlight the link between H_k and $\dot{Q}_k$ and can be written as follows :

$$H_1 = 0, \tag{1}$$

$$\forall k \in [2, N+1], \quad h_c H_k = -\sum_{i=1}^{k-1} \dot{Q}_i, \tag{2}$$

where h_c is the conductor width.

2) In the conductor layers: Considering hypothesis v) and vii),

$$\nabla \times \mathbf{E} = -\mu_0 \frac{\partial \mathbf{H}}{\partial t} \tag{3}$$

$$\nabla \times \mathbf{H} = \mathbf{j} \tag{4}$$

$$\mathbf{j} = \sigma \mathbf{E}, \tag{5}$$

where σ the conductor conductivity. Based on hypothesis iii), the magnetic field $\mathbf{H}$ only has a z-component. Using Equation (3) it implies that the electric field strength $\mathbf{E}$ only has a y-component. The invariance hypothesis along the y- and z-axis iv) and iii) implies that both fields $\mathbf{E}$ and $\mathbf{H}$ are only function of x. Thus, Equations (3)-(5) become in the k^{th} conductor layer:

$$\frac{dE_{y_k}}{dx_k} = -j\omega\mu_0 H_{z_k} \tag{6}$$

$$-\frac{dH_{z_k}}{dx_k} = \sigma E_{y_k}, \tag{7}$$

giving the Helmoltz differential equation:

$$\frac{d^2 H_{z_k}}{dx_k^2} = j\omega\mu_0\sigma H_{z_k}. \tag{8}$$

Its general solution is

$$H_{z_k}(x_k) = H_{1_k} e^{\alpha x_k} + H_{2_k} e^{-\alpha x_k}, \tag{9}$$

where α is the complex wave number,

$$\alpha = \sqrt{j\omega\mu_0\sigma} = \frac{1+j}{\delta} \tag{10}$$

and δ the skin depth,

$$\delta = \sqrt{\frac{2}{\mu_0\sigma\omega}}. \tag{11}$$

H_{1_k} and H_{2_k} are integration constants that can be evaluated from the boundary conditions (see inset in Fig. 2):

$$H_{z_k}(x_k = 0) = H_k, \tag{12}$$

$$H_{z_k}(x_k = e_c) = H_{k+1}, \tag{13}$$

where e_c is the conductor thickness. It derives :

$$H_{1_k} = \frac{H_{k+1} - H_k e^{-\alpha e_c}}{e^{\alpha e_c} - e^{-\alpha e_c}}, \tag{14}$$

$$H_{2_k} = \frac{H_k e^{\alpha e_c} - H_{k+1}}{e^{\alpha e_c} - e^{-\alpha e_c}}. \tag{15}$$

Finally, in the k[th] conductor, the magnetic field distribution is expressed as follows:

$$H_{z_k}(x_k) = \frac{H_{k+1} - H_k e^{-\alpha e_c}}{e^{\alpha e_c} - e^{-\alpha e_c}} e^{\alpha x_k} + \frac{H_k e^{\alpha e_c} - H_{k+1}}{e^{\alpha e_c} - e^{-\alpha e_c}} e^{-\alpha x_k} \tag{16}$$

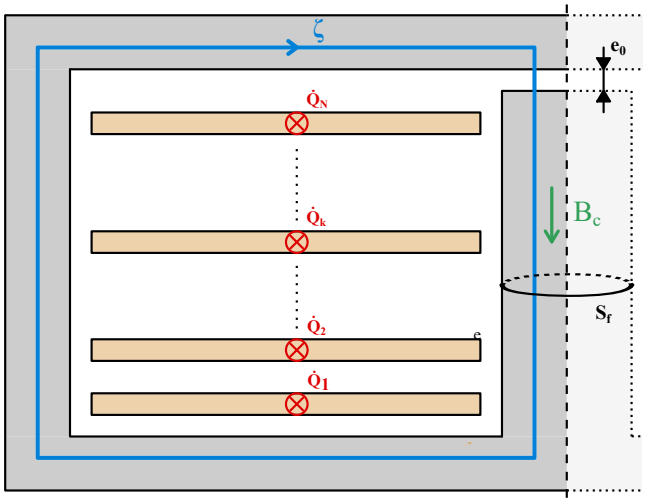

Fig. 3: Definition of the Ampère closed path used to calculate the magnetising energy in the transformer core.

C. Joule losses, leakage energy and magnetizing energy

Combining the magnetic field in the conductors (16) and equations (1) and (2), the total Joule losses P_J and the total magnetic leakage energy E_{lk} (stored in the winding window) are calculated as functions of the currents vector $\dot{\mathrm{Q}} = [\dot{Q}_1, ..., \dot{Q}_N]^T$. These relations are published in the scientific literature [21], [22]. They are detailed and rewritten in matrix form in the appendix . This leads to the following equations:

$$P_J = \dot{\mathrm{Q}}^\dagger \mathrm{R} \dot{\mathrm{Q}}, \tag{17}$$

$$E_{lk} = \frac{1}{2} \dot{\mathrm{Q}}^\dagger \mathrm{L_{lk}} \dot{\mathrm{Q}} \tag{18}$$

where R and $\mathrm{L_{lk}}$ are $N \times N$ resistance and leakage inductance matrix, respectively, and † is the transpose conjugate operator.

The magnetizing energy, which is stored in the magnetic core and the air gap, represents the magnetic coupling between the windings. The application of the Ampere theorem on the closed path ζ defined on Fig. 3 gives the magnetic induction amplitude B_c along the path:

$$B_c = \left(\frac{\mu_0}{\frac{d_m}{\mu_r} + e_0} \right) \sum_{k=1}^{N} \dot{Q}_k. \tag{19}$$

with d_m the mean length of a magnetic field line, e_0 the air gap thickness and μ_r the relative permeability of the core. The magnetizing energy can then be calculated by integration of the magnetic energy density in the core and the air gap:

$$E_\mu = \frac{\mu_0 S_f}{2\left(\frac{d_m}{\mu_r} + e_0\right)} \left| \sum_{k=1}^{N} \dot{Q}_k \right|^2 = \frac{1}{2} \dot{\mathrm{Q}}^\dagger \mathrm{L}_\mu \dot{\mathrm{Q}}, \tag{20}$$

with S_f the effective flux area of the core and L_μ the magnetizing inductance matrix:

$$\mathrm{L}_\mu = \frac{\mu_0 S_f}{\left(\frac{d_m}{\mu_r} + e_0\right)} \begin{bmatrix} 1 & \dots & 1 \\ \vdots & \ddots & \vdots \\ 1 & \dots & 1 \end{bmatrix}_{N \times N}. \tag{21}$$

D. AC resistance and leakage inductance

AC resistance R_{AC} and AC leakage inductance L_{AC} are defined from P_J and E_{lk}, respectively. Consequently, they both depend (through the variable $\dot{Q}$) on the current distribution in the parallel connected windings. Considering that a current I_0 flows through one of the windings, R_{AC} and L_{AC} (referred to that winding) are expressed as follows :

$$R_{AC} = \frac{P_J}{I_0^2} = \frac{\dot{\mathrm{Q}}^{\dagger}\mathrm{R}\dot{\mathrm{Q}}}{I_0^2}, \tag{22}$$

and,

$$L_{AC} = \frac{2E_{lk}}{I_0^2} = \frac{\dot{\mathrm{Q}}^{\dagger}\mathrm{L_{lk}}\dot{\mathrm{Q}}}{I_0^2}. \tag{23}$$

Thus, to estimate the R_{AC} and L_{AC} values, the unknown vector $\dot{\mathrm{Q}}$ must be identified.

E. An energetic resolution method

In 2003, Wei Chen proposed the only method allowing to explicitly and analytically express the system of equations verified by the currents flowing through the parallel connected windings [19]. The system of linear equations in $\dot{Q}$ is constructed by solving the Faraday theorem locally on N well-chosen contours. This implies in particular to integrate the magnetic flux density on the surfaces associated to these contours. This represents a significant additional physical modeling effort, useless to address the current objectives, i.e. R_{ac} and L_{ac} assessment.

The present paper suggests a more global approach based on an energy resolution method. It enables to construct the linear system on $\dot{\mathrm{Q}}$ only using the losses and stored energies in the transformer, i.e. P_J, E_{lk} and E_μ (Equations (17), (18) and (20)). For this purpose, the Lagrangian equations of the systems dynamics, detailed in the section III, enable to do without the complex resolution of the Maxwell-Faraday law proposed by Wei Chen. Conversely the suggested energy approach permits to fully exploit the R_{AC} and L_{AC} expressions, which are well-established and, by definition, mandatory.

III. Procedure for applying the Euler-Lagrange dynamics equations to the transformer

The Euler-Lagrange equations are fundamental laws of system dynamics. They apply to any type of physical system: mechanical, electrical or electromechanical. The Euler-Lagrange equations for electrical systems are well established in the literature [25], [26]. In this paper, they are only applied to the "planar transformer" electrical system to obtain its dynamic equations and thus the current distribution in the parallel windings. For more details on the physical meaning and the demonstration of the Euler-Lagrange equations from the principle of least action, the reader can consult the following references [26], [27], [28], [29]. The general form of Euler-Lagrange equations for electrical systems is [25]:

$$\begin{cases} \frac{d}{dt}\left(\frac{\partial \mathcal{L}}{\partial \dot{\mathrm{Q}}}\right) - \frac{\partial \mathcal{L}}{\partial \mathrm{Q}} = -\frac{\partial \mathcal{D}}{\partial \dot{\mathrm{Q}}} + \mathrm{A}\lambda + \mathcal{U} \\ \mathrm{A}^T\dot{\mathrm{Q}} = \mathcal{I}, \end{cases} \tag{24}$$

where:

- $\mathrm{Q}^T = [Q_1 \dots Q_N]$ represents the N coordinates of the system state. In the case of an electromagnetic system, Q corresponds to the electrical charge and its time derivative $\dot{\mathrm{Q}}$ is the electric current.
- $\mathcal{L}(\mathrm{Q}, \dot{\mathrm{Q}})$, the system lagrangian is a scalar function defined as the difference between the kinetic energy of the system $\mathcal{T}(\mathrm{Q}, \dot{\mathrm{Q}})$ (magnetic energy) and its potential energy $\mathcal{V}(\mathrm{Q})$ (electric energy):
$$\mathcal{L}(\mathrm{Q}, \dot{\mathrm{Q}}) = \mathcal{T}(\mathrm{Q}, \dot{\mathrm{Q}}) - \mathcal{V}(\mathrm{Q}). \tag{25}$$
Physical details on the link between kinetic and magnetic energy, and potential and electric energy are given in [26].
- $\mathcal{D}(\dot{\mathrm{Q}})$ is the Rayleigh dissipation function. It is defined as half of the power dissipated by friction, which, in this case, corresponds here to the Joule losses.
- The generalized force vector $\mathcal{U}^T = [\mathcal{U}_1, \dots, \mathcal{U}_N]$ includes the non-conservative forces (i.e. voltage sources) apart from the friction forces (i.e. Joule effect).
- The matrices A^T and $\mathcal{I}$ represent the m internal constraints on the coordinates such as series connection of turns and currents sources (given in $\mathcal{I}$). Their developed form is given below:
$$\sum_k a_{lk}\dot{Q}_k + \mathcal{I}_l = 0, \quad l \in [1, m], \tag{26}$$
with,
$$\begin{aligned} \mathrm{A}^T &= (a_{lk}) \qquad \text{size } m \times N \\ \mathcal{I} &= (\mathcal{I}_l) \qquad \text{size } m \times 1. \end{aligned} \tag{27}$$
- λ is a vector composed of m additional unknowns. It enables to obtain a linear system with $N+m$ unknowns and $N+m$ equations according to the mathematical method of Lagrange multiplier. In the case of transformers, λ coordinates physically correspond to the unknown internal voltages (voltages at the terminals of the series-connected turns) that guarantee the constraints imposed to the system (same current in these specific turns). More details on Lagrange multiplier are given in [30], [31].

In this article, this energy formulation is only used as a mathematical tool to build the linear system on $\dot{\mathrm{Q}}$. Its application on the concrete example of a transformer shows how systematic and straightforward this method can be. The procedure is detailed below.

A. Calculate the Lagrangian $\mathcal{L}$

In this study, the electric energy, which is related to the capacitive coupling between winding turns, is negligible at the operating frequencies of the transformer. And this model does not attempt to account for capacitive effects at higher frequencies. The potential energy function is then zero, $\mathcal{V}(\mathrm{Q}) = 0$, and the Lagrangian scalar function is limited to the sum of the kinetic energies E_{lk} and E_μ :

$$\mathcal{L}(\mathrm{Q}, \dot{\mathrm{Q}}) = \mathcal{T}(\mathrm{Q}, \dot{\mathrm{Q}}) = \frac{1}{2}\dot{\mathrm{Q}}^{\dagger}\left(\mathrm{L}_\mu + \mathrm{L_{lk}}\right)\dot{\mathrm{Q}}. \tag{28}$$

B. Calculate the dissipation function $\mathcal{D}$

The dissipation function is defined as half of the power dissipated by friction, i.e. the Joule losses:

$$\mathcal{D}(\dot{\mathrm{Q}}) = \frac{1}{2}\dot{\mathrm{Q}}^{\dagger}\mathrm{R}\dot{\mathrm{Q}}. \tag{29}$$

C. Define the voltage sources in $\mathcal{U}$

One or more winding turns may be connected to a voltage source. If so, the complex amplitude of this voltage source is specified in a force vector $\mathcal{U}$, size N, in the corresponding line(s).

D. Build the constraint matrix A^T and $\mathcal{I}$

The A^T matrix represents the m equations constraining the dynamic of the state variables. In the transformer case, these equations only reflects the electrical connections between the series connected winding turns. Indeed, the currents in the turns connected in parallel are not constrained by definition. Noting $\mathcal{S}$ a winding with series connected turns, the following constraint equations must be considered :

$$\forall\{i,j\} \in \mathcal{S}^2, \quad \dot{Q}_i = \dot{Q}_j \tag{30}$$

Any current sources are represented in the $\mathcal{I}$ vector. A concrete example is detailed in section IV.

E. Derive $\mathcal{L}$ and $\mathcal{D}$ to get the linear system on $\dot{\mathrm{Q}}$

The equation system on $\dot{\mathrm{Q}}$ derives from the Euler-Lagrange equations (24). First, the scalar functions $\mathcal{L}$ and $\mathcal{D}$ are derived using the matrix derivation rules and considering that L_μ, L_{lk} and R are symmetric matrix:

$$\frac{\partial \mathcal{L}}{\partial \dot{\mathrm{Q}}} = \frac{1}{2}\frac{\partial\left[\dot{\mathrm{Q}}^{\dagger}(\mathrm{L}_\mu + \mathrm{L}_{\mathrm{lk}})\dot{\mathrm{Q}}\right]}{\partial \dot{\mathrm{Q}}} = (\mathrm{L}_\mu + \mathrm{L}_{\mathrm{lk}})\dot{\mathrm{Q}}, \tag{31}$$

$$\frac{\partial \mathcal{L}}{\partial \mathrm{Q}} = 0, \tag{32}$$

$$\frac{\partial \mathcal{D}}{\partial \dot{\mathrm{Q}}} = \frac{1}{2}\frac{\partial\left[\dot{\mathrm{Q}}^{\dagger}\mathrm{R}\dot{\mathrm{Q}}\right]}{\partial \dot{\mathrm{Q}}} = \mathrm{R}\dot{\mathrm{Q}}. \tag{33}$$

Thus, the Euler-Lagrange equations (24) applied to the planar transformer in harmonic regime are reduced to a linear system of $N+m$ equations and $N+m$ unknowns:

$$\begin{cases} (\mathrm{R} + j\omega(\mathrm{L}_\mu + \mathrm{L}_{\mathrm{lk}}))\dot{\mathrm{Q}} = \mathrm{A}\lambda + \mathcal{U} \\ \\ \mathrm{A}^T\dot{\mathrm{Q}} = \mathcal{I}. \end{cases} \tag{34}$$

Where the unknown vector $\mathrm{X}_{(N+m)\times 1}$ is defined as,

$$\mathrm{X} = \begin{bmatrix} \dot{\mathrm{Q}} \\ \lambda \end{bmatrix}. \tag{35}$$

Finally the linear system is expressed in matrix form (36):

$$\begin{bmatrix} (\mathrm{R} + j\omega(\mathrm{L}_\mu + \mathrm{L}_{\mathrm{lk}})) & -\mathrm{A} \\ \mathrm{A}^T & (0)_{m\times m} \end{bmatrix} \mathrm{X} = \begin{bmatrix} \mathcal{U} \\ \mathcal{I} \end{bmatrix}. \tag{36}$$

IV. Case study and validation

A. Case-study description

Fig.1 shows the planar transformer that has been manufactured. It is composed of an E-I magnetic core and a ten-layer PCB. The physical and geometrical parameters are presented in Table I. In the ten-layer PCB, the five first layers A are series connected to form a five-turn primary winding and the last five layers B are parallel connected to form a one-turn secondary winding. This winding configuration is called *non-interleaved* and is noted as follows :

$$A - A - A - A - A - B - B - B - B - B$$

All the 5 secondary layers B are connected in parallel, meaning that the secondary current flow is not constrained in these layers. Conversely, the primary winding is connected to a voltage source U_0 and all its winding turns A are connected in series, meaning that the primary current flow is constrained by the equations (30). From these considerations can be deduced the linear system of constraints (37) and the voltage source vector, i.e. the matrix A, $\mathcal{I}$ and $\mathcal{U}$.

$$\overbrace{\begin{pmatrix} 1 & -1 & 0 & 0 & 0 & 0 & 0 & 0 & 0 & 0 \\ 0 & 1 & -1 & 0 & 0 & 0 & 0 & 0 & 0 & 0 \\ 0 & 0 & 1 & -1 & 0 & 0 & 0 & 0 & 0 & 0 \\ 0 & 0 & 0 & 1 & -1 & 0 & 0 & 0 & 0 & 0 \end{pmatrix}}^{\mathrm{A}^T} \dot{\mathrm{Q}} = \overbrace{\begin{pmatrix} 0 \\ 0 \\ 0 \\ 0 \end{pmatrix}}^{\mathcal{I}}, \tag{37}$$

and,

$$\mathcal{U} = \begin{bmatrix} U_0 & 0 & \dots & 0 \end{bmatrix}^T \tag{38}$$

B. Results and validation

A short-circuit test on secondary winding is considered to validate the model. Fig. 4a and 4b show the results of AC resistance and leakage inductance measurements, both referred to the primary side. They were carried out with an impedance analyzer Keysight E4990A (Fig. 5), the primary side being connected to the impedance analyzer while the

TABLE I: Transformer parameters

Parameter	**Symbol**	**Value**
Voltage ratio	-	5
Conductor thickness	e_c	190 µm
Insulator thickness	ei	see below (*)
Conductor width	h_c	19.5 mm
Coil mean turn length	L_c	176 mm
Core type	-	E58/11/38
Core material	-	Ferrite 3C95
Core initial permeability	μ_r	3000
Air gap	e_0	180 µm
Effective flux area	S_f	310 mm²

(*) ei gathers the $N+1$ insulator thicknesses between winding turns defined in Fig. 2, in millimeter : 5 - 0.31 - 0.22 - 0.33 - 0.22 - 0.33 - 0.22 - 0.33 - 0.22 - 0.31 - 5

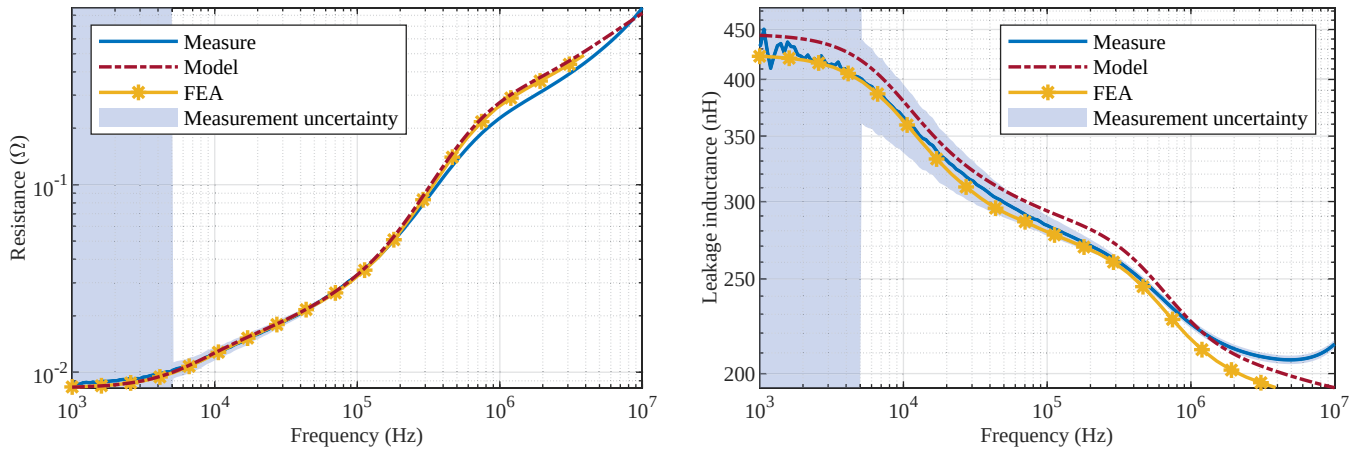

(a) AC resistance R_{AC} vs. frequency

(b) Leakage inductance L_{AC} vs. frequency

Fig. 4: Comparison between measure, 2D FEA simulations and the analytical model for the non-interleaved configuration : A-A-A-A-A-B-B-B-B-B. The blue colored zones corresponds to the accuracy of the measuring instruments.

secondary side is shorted. The impedance measurement accuracy, extracted from the analyzer datasheet, is represented as well. At low frequencies, i.e. between 1 kHz and 5 kHz, the analyzer accuracy is not specified. Nonetheless, the DC resistance value was confirmed with a digital low resistance ohmmeter (Megger DLRO10HD).

R_{AC} and L_{AC} are also computed using the proposed analytical model and a Finite Element Analysis (FEA) carried out in 2D using FEMM software. For comparison purposes, these computation results are displayed in the same graphs (Fig. 4a and 4b).

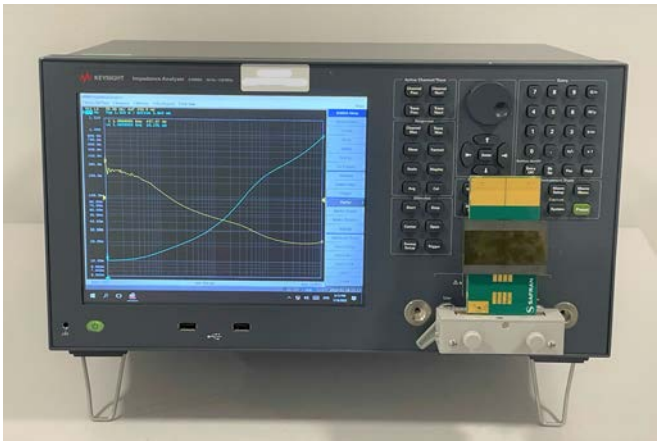

Fig. 5: Photograph of the experimental set-up.

The analytical model estimations of both R_{AC} and L_{AC} are consistent with both measurements and FEA simulations over the whole frequency range. However, a few minor deviations can be observed and explained:

- Above a few MHz, the transformer behavior is influenced by a resonance occurring at 30 MHz. This explains the deviation in the measured leakage inductance.
- A discrepancy between measurement and 2D models (both analytical and FEA) can be noticed in Fig. 4a around 1 MHz. These 2D models cannot represent perfectly the actual 3D transformer (Fig. 1). Many elements such as winding ends, vias or connectors are not considered.

Note that FEA simulations have also been conducted and compared to the analytical model for many other winding configurations and geometries. Corresponding results are shown in Figure 6 for the following three configurations: A-B-A-B-A-B-A-B-A-B (fully interleaved), A-B-B-A-A-B-B-A-A-B (partially interleaved 1) and A-A-B-B-B-A-A-A-B-B (partially interleaved 2). AC resistance and leakage inductance estimation match just as well as the ones in Fig. 4a and 4b, which validates the proposed analytical model. No significant deviation can be highlighted for the AC resistance, while the analytical model always overestimates the AC leakage inductance by a few percent compared to the finite element simulations. This may be due to the fact that in the analytical model the field is assumed to be completely confined between the conductors. In reality, it spreads out a little at the edges, between the winding and the ferrite, which slightly reduces the amplitude of the magnetic field in the insulating layers and thus the leakage energy.

C. Analysis and discussions

In addition to its accuracy, the suggested analytical model provides an alternative understanding of the skin and proximity effects, as well as the current distribution in parallel connected winding turns. The following observations are based on Fig. 7a and 7b which respectively depict the Joule loss density in the conductor layers and the magnetic energy density distribution in the winding window at different frequencies, respectively.

First, Fig. 7b reveals the magnetic coupling between the transformer windings since the magnetic field ends up canceling after the tenth turn. This means that the sum of the currents is zero, which is expected in a transformer. The equation (20) indicates that a cancellation of the sum of the

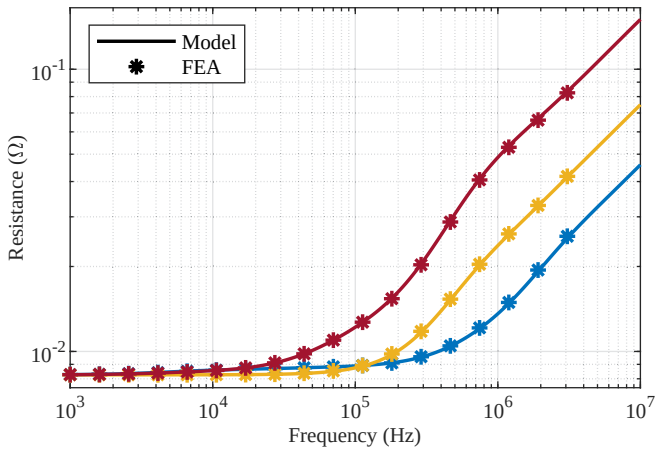

(a) AC resistance R_{AC} vs. frequency.

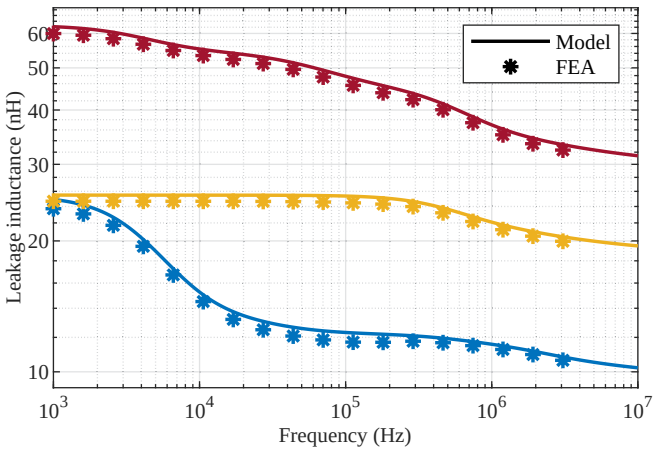

(b) Leakage inductance L_{AC} vs. frequency.

Fig. 6: Comparison between 2D FEA simulations (asterisk markers) and the analytical model (solid lines) for the configurations A-B-A-B-A-B-A-B-A-B (fully interleaved in blue), A-B-B-A-A-B-B-A-A-B (partially interleaved 1 in yellow) and A-A-B-B-B-A-A-A-B-B (partially interleaved 2 in red).

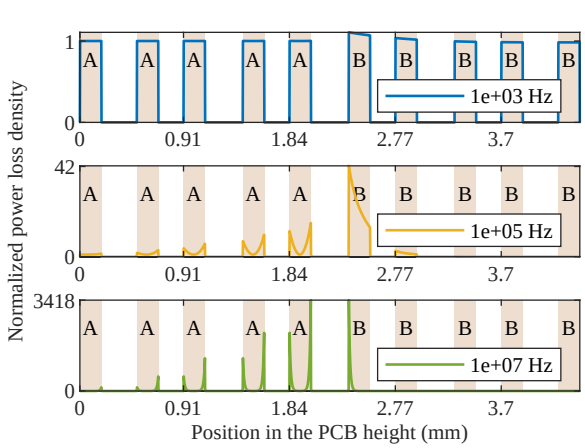

(a) The Joule losses density is normalised in comparison with the power losses density generated by an homogeneous current I_0 flowing in one winding turn.

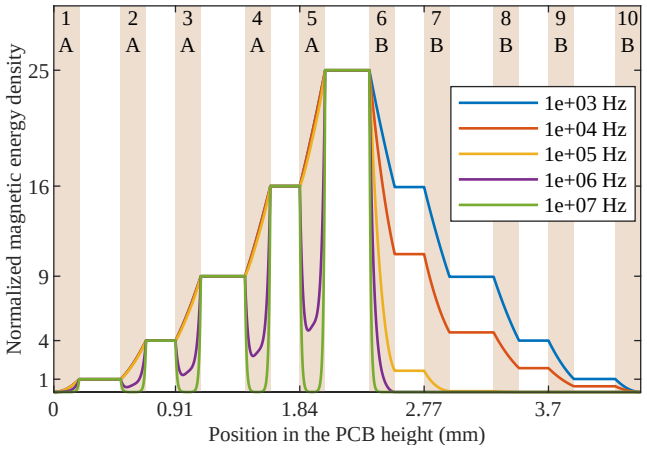

(b) The magnetic leakage energy density is normalised in comparison with the energy density generated by one winding turn crossed by a current I_0.

Fig. 7: Joule losses density distribution and magnetic leakage energy density distribution at different frequencies. The 10 copper layers regions are coloured in pale orange, the insulation layers regions are not coloured.

currents also corresponds to the cancellation of the magnetizing energy. Thus, it appears that the induced currents in the secondary winding tend to cancel and therefore minimize the magnetizing energy.

Second, in Fig. 7a, note that at low frequencies, the current density tends to be uniform in all the turns, which minimizes the Joule losses and thus R_{AC}. On the contrary, at high frequencies, the current density is highly localized on the turns horizontal edges, in such a way that tends to minimise the magnetic energy in the winding window and thus L_{AC}. At intermediate frequencies, the current density distribution seems to be a compromise between minimizing the AC resistance and minimizing the AC leakage inductance.

These observations are consistent with Euler-Lagrange equations of dynamics which are based on the principle of least action. In electromagnetism and more precisely in electronics, this principle states that *the current follows the path of least impedance*. The linear system (36) mathematically reflects this principle. Its formulation is analogous to minimizing the transformer impedance under linear constraints and using Lagrange multipliers method, a standard minimization method [31]. In the present industrial context where the need for high frequency transformers with high current parallel connected windings is rising, this *least impedance* principle can help designing the windings and choosing the appropriate configuration. The following general recommendations can be deduced and followed.

D. Design recommendation

To optimize the use of materials and limit the power losses, the current must be as uniform as possible in the copper

layers. Two levels for improvement can be identified. First, the copper layers thickness e must be chosen in accordance with the skin depth δ. A relative skin depth $\Delta = e/\delta$ of 1 to 1,5 is a standard choice [32]. Second, the AC leakage inductance should be kept small so that $R_{AC} \sim j\omega L_{AC}$ at the operating frequency. Thus, the current density distribution is governed by the minimization of Joule losses and remains uniform.

The main lever to reduce the leakage inductance is to interleave the windings, which is well known in the literature [23]. Figure 8 shows the leakage magnetic energy density in the winding window for the four winding configurations considered in this paper. These curves are plotted for a frequency of 300 kHz, giving a relative skin depth of 1.6. It is clear that the more interleaved the windings are, the lower the magnetic energy density in the insulation layers, and thus the lower the leakage inductance. Table II lists the corresponding inductance values and the normalized AC resistance. For this transformer, which geometry is defined in Table I, the fully interleaved configuration generates 10 times less losses than the non-interleaved, a huge gain.

However, there is a trade-off between the leakage inductance and the parasitic capacitance of the windings, especially for planar technology. Reducing the leakage inductance usually means increasing the parasitic capacitance, and the latter can seriously affect the magnetic performance of the component [3], [9]. Also, in some specific cases, the inductance function is integrated in the transformer. A precise value of the leakage inductance is then desired. For these reasons, the fully interleaved configuration is not always the solution. It is necessary to find the configuration that fits the specifications, the one that minimizes the Joule losses while respecting all the constraints. It is in this optimization process that the presented analytical model shows its value.

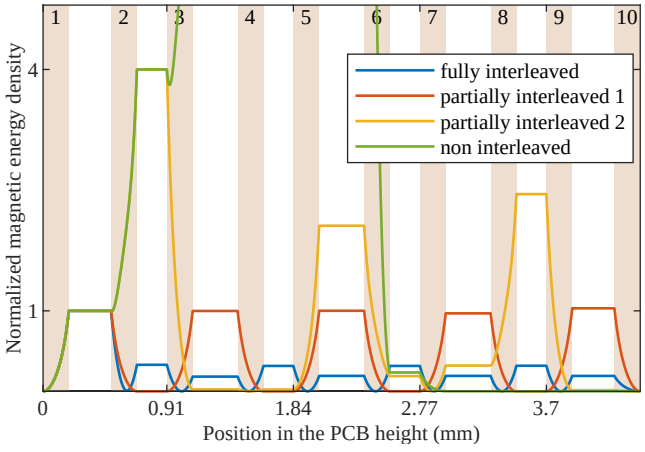

Fig. 8: Magnetic leakage energy density distribution for different winding configurations at 300 kHz. It is normalised in comparison with the energy density generated by one winding turn crossed by a current I_0. The 10 copper layers regions are coloured in pale orange, the insulation layers regions are not coloured.

TABLE II: Configurations comparison at 300 kHz.

Configuration	$\mathbf{R_{AC}/R_{DC}}$	$\mathbf{L_f}$ (nH)
Fully interleaved	1.16	12.1
Partially interleaved 1	1.44	24.6
Partially interleaved 2	2.53	43.5
Non-interleaved	11.0	271

E. User's guide to the method

Below are the steps to follow to numerically solve the linear system (36) and estimate the AC resistance and leakage inductance of a planar transformer using the analytical equations presented in this paper. These steps can be integrated into an automatic tool.

- Choose any numerical calculation platform.
- Define the geometrical parameters of the transformer (length, width, thickness of conductor layers ...), the material properties (permittivity, conductivity) and the test frequency.
- Code the matrices R, L_{lk}, and L_μ using the formulas given in Equations (48), (55) and (21) to get their numerical value. Note that P, A_J, B_J, Δ, A_{lk}, B_{lk} are given by Equations (39),(42), (43), (44), (51) and (52).
- Define your winding configuration, identify the position of the series-connected turns and construct the constraint matrix A and the voltage source vector $\mathcal{U}$ following the approach described in the IV-A section.
- From these matrices, construct and solve numerically the linear system (36). At this stage, the current flowing through all the turns is known.
- Deduce the value of the AC resistance and AC inductance using the equations (22) and (23). Note that the current I_0 is the current flowing through the primary winding.
- Finally, check that the effects of the parasitic capacitance are negligible: the resonance frequency of this capacitance with the leakage inductance must be much higher than the frequency at which R_{AC} and L_{AC} have been calculated. This parasitic capacitance can for example be estimated using the analytical model proposed by Ouyang [9].

Note that this model is quite suitable for multi-winding transformers. The procedure to follow is similar to the two-winding case. It consists in defining the series connected turns in the constraint matrix A. Then, one of the windings is loaded by a voltage source (to be entered in the vector $\mathcal{U}$). The others are either open-circuited (zero current constraint to be added in A), or short-circuited (no constraint to be added).

For example, the case study presented in this article deals with a transformer with a secondary winding comprising 5 turns connected in parallel and short-circuited. It could be equally considered as 5 windings made of one short-circuited

turn. These two views are equivalent and are processed in the same way.

V. Conclusion

In high turns ratio transformers, high currents flow into the low-voltage winding. Connecting several identical turns in parallel is a standard solution to share the current and reduce the Joule losses. Unfortunately, in AC, the currents in these parallel turns are not necessarily well balanced. This phenomenon is particularly marked at high frequencies, such as those currently used in isolated DC/DC power supplies (100 kHz to 1 MHz). The challenge is to provide the engineer with an efficient analytical tool, allowing him to quickly access a near-optimal design. This solution can then be refined with a 3D simulation tool and the manufacture of a prototype.

Based on an energy approach, an innovative and original tool is proposed. It enables the calculation of the currents distribution in the parallel connected turns of a planar transformer as well as the two macroscopic parameters which are the AC resistance R_{AC} and the leakage inductance L_{AC}, at different working frequencies. These two key parameters determine the performance of the transformer in its environment and enables to estimate whether or not the current choice of geometrical parameters is optimal or not. Furthermore, note that this new technique gives an analytical answer based only on the knowledge of the magnetic properties and the geometrical dimensions of the core material, as well as the geometrical design of the different turns in the winding window.

This approach can be implemented in an automatic tool and therefore enables quick answers with any type of transformer and on any numerical calculation platform. The related very short calculation time offers the ability to test many different parameters or configurations and choose the best design and sizing. Moreover, since the method is based on general physical principles, it provides an explicit and clear reading of the results found. Understanding the trade-off between Joule losses and magnetic leakage energy stored in the winding window guides the transformer designer in his iterations, allowing him to quickly reach an optimal solution integrating the other design constraints.

Appendix
Energy calculations

A. Transfer matrix between magnetic field and current

In the literature, many articles give the analytical expression of the Joule losses and/or of the total leakage energy stored in the winding window [20], [21], [22], [23]. They are calculated considering the same assumptions as those presented in the present paper, and have been validated by FEA simulations and/or experimentally [17], [19], [22], [23]. Most of the time, they are first calculated as a function of the magnetic field amplitude H_k in the insulation layers which is mathematically easier. Next, a variable change is performed to get the expressions of the power losses and the leakage energy as a function of the current flowing in the winding turns.

Obviously, this paper follows a similar approach. A transfer matrix P enables to define the relationship between vectors $\mathrm{H} = [H_1, ..., H_{N+1}]^T$ and $\dot{\mathrm{Q}}$. This matrix corresponds to equations (1) and (2) :

$$\mathrm{H} = \mathrm{P}\dot{\mathrm{Q}}, \quad \text{where} \quad \mathrm{P} = -\frac{1}{h_c}\begin{pmatrix} 0 & \dots & 0 \\ 1 & & (0) \\ \vdots & \ddots & \\ 1 & \dots & 1 \end{pmatrix}_{(N+1)\times(N)}. \tag{39}$$

B. Joule losses P_J

The Joule losses P_k in the k^{th} copper layer is,

$$P_k = L_c \iint_{\Omega_k} \sigma |E_y|^2 dx_k dz_k = \frac{L_c h_c}{\sigma} \int_0^e \left|\frac{dH_z}{dx}\right|^2 dx_k, \tag{40}$$

The total Joule losses P_J can be calculated by inserting Equation (9) in Equation (40), then solving the integral and summing the contribution of all copper layers,

$$P_J = \sum_{k=1}^{N} \frac{L_c h_c}{\sigma\delta}\Big[A_J(\Delta)\left(|H_k|^2 + |H_{k+1}|^2\right) - B_J(\Delta)\,\Re\left(H_k^* H_{k+1}\right)\Big] \tag{41}$$

where,

$$A_J(\Delta) = \frac{\sinh(2\Delta) + \sin(2\Delta)}{\cosh(2\Delta) - \cos(2\Delta)}, \tag{42}$$

$$B_J(\Delta) = 4\frac{\cos(\Delta)\sinh(\Delta) + \cosh(\Delta)\sin(\Delta)}{\cosh(2\Delta) - \cos(2\Delta)} \tag{43}$$

$$\Delta = e/\delta. \tag{44}$$

Noticing that,

$$|H_k|^2 = H_k H_k^*, \tag{45}$$

that,

$$\Re\left(H_k^* H_{k+1}\right) = \frac{1}{2}\left(H_k^* H_{k+1} + H_k H_{k+1}^*\right), \tag{46}$$

and using the transfer matrix P given in Equation (39), P_J can be expressed in a matrix form:

$$P_J = \dot{\mathrm{Q}}^{\dagger}\mathrm{R}\dot{\mathrm{Q}}, \tag{47}$$

where $\dagger$ is the transpose conjugate operator and R is an $N \times N$ matrix which has the following form:

$$\mathrm{R} = \frac{L_c h_c}{\sigma\delta}\mathrm{P}^{\dagger}\underbrace{\begin{pmatrix} A_J & -\frac{B_J}{2} & & & (0) \\ -\frac{B_J}{2} & 2A_J & -\frac{B_J}{2} & & \\ & \ddots & \ddots & \ddots & \\ & & -\frac{B_J}{2} & 2A_J & -\frac{B_J}{2} \\ (0) & & & -\frac{B_J}{2} & A_J \end{pmatrix}}_{\text{Size } (N+1)\times(N+1)}\mathrm{P}. \tag{48}$$

C. Leakage magnetic energy E_{lk}

1) In the copper layers: The leakage magnetic energy E_{lk,c_k} in the k^{th} conductor layer is,

$$E_{lk,c_k} = L_c \int_{\Omega_k} \frac{\mu_0 |H_z|^2}{2} d\Omega_k = \frac{\mu_0 L_c h_f}{2} \int_0^e |H_{z_k}(x)|^2 dx \tag{49}$$

The total leakage magnetic energy $E_{lk,c}$ in the conductor layers can be calculated by solving the integral and summing the contribution of all copper layers :

$$E_{lk,c} = \frac{L_c h_c}{2\sigma\delta\omega} \sum_{k=1}^{N} \Big[A_m(\Delta) \left(|H_k|^2 + |H_{k+1}|^2 \right) - B_m(\Delta) \Re \left(H_k^* H_{k+1} \right) \Big] \tag{50}$$

where,

$$A_{lk}(\Delta) = \frac{\sinh(2\Delta) - \sin(2\Delta)}{\cosh(2\Delta) - \cos(2\Delta)} \tag{51}$$

$$B_{lk}(\Delta) = 4 \frac{\cos(\Delta)\sinh(\Delta) - \cosh(\Delta)\sin(\Delta)}{\cosh(2\Delta) - \cos(2\Delta)}. \tag{52}$$

2) In the insulation layers: The magnetic field being uniform inside the isolation layers, the magnetic energy $E_{lk,iso}$ inside the insulation layers is more easily expressed :

$$E_{lk,iso} = \sum_{k=1}^{N+1} \frac{\mu_0 L_c h_f e i_k}{2} |H_k|^2 \tag{53}$$

3) The total magnetic leakage energy: The total magnetic leakage energy can be expressed as a matrix product:

$$E_{lk} = \frac{1}{2} \dot{\mathrm{Q}}^{\dagger} \mathrm{L_{lk}} \dot{\mathrm{Q}}, \tag{54}$$

where $\mathrm{L_{lk}} = \mathrm{P}^{\dagger} \mathrm{M} \mathrm{P}$ is a $N \times N$ matrix, and M is an $(N+1) \times (N+1)$ matrix defined as follows :

$$\mathrm{M} = \frac{L_c h_c}{\sigma\delta\omega} \begin{pmatrix} A_{lk} & -\frac{B_{lk}}{2} & & & (0) \\ -\frac{B_{lk}}{2} & 2A_{lk} & -\frac{B_{lk}}{2} & & \\ & \ddots & \ddots & \ddots & \\ & & -\frac{B_{lk}}{2} & 2A_{lk} & -\frac{B_{lk}}{2} \\ (0) & & & -\frac{B_{lk}}{2} & A_{lk} \end{pmatrix} + \mu_0 L_c h_c \begin{pmatrix} ei_1 & & & (0) \\ & ei_2 & & \\ & & \ddots & \\ (0) & & & ei_{N+1} \end{pmatrix} \tag{55}$$

REFERENCES

[1] J. S. Ngoua Teu Magambo, R. Bakri, X. Margueron, P. Le Moigne, A. Mahe, S. Guguen, and T. Bensalah, "Planar Magnetic Components in More Electric Aircraft: Review of Technology and Key Parameters for DC–DC Power Electronic Converter," *IEEE Transactions on Transportation Electrification*, vol. 3, pp. 831–842, Dec. 2017.

[2] X. Zhou, B. Sheng, W. Liu, Y. Chen, L. Wang, Y.-F. Liu, and P. C. Sen, "A High-Efficiency High-Power-Density On-Board Low-Voltage DC–DC Converter for Electric Vehicles Application," *IEEE Transactions on Power Electronics*, vol. 36, pp. 12781–12794, Nov. 2021.

[3] Z. Ouyang and M. A. E. Andersen, "Overview of Planar Magnetic Technology—Fundamental Properties," *IEEE Transactions on Power Electronics*, vol. 29, pp. 4888–4900, Sept. 2014.

[4] S. R. Cove, M. Ordonez, F. Luchino, and J. E. Quaicoe, "Applying Response Surface Methodology to Small Planar Transformer Winding Design," *IEEE Transactions on Industrial Electronics*, vol. 60, pp. 483–493, Feb. 2013.

[5] C. Buccella, C. Cecati, and F. de Monte, "A Coupled Electrothermal Model for Planar Transformer Temperature Distribution Computation," *IEEE Transactions on Industrial Electronics*, vol. 55, pp. 3583–3590, Oct. 2008.

[6] M. A. Saket, M. Ordonez, and N. Shafiei, "Planar Transformers With Near-Zero Common-Mode Noise for Flyback and Forward Converters," *IEEE Transactions on Power Electronics*, vol. 33, pp. 1554–1571, Feb. 2018.

[7] K. R. de Faria, D. Sadarnac, C. Karimi, L. Bendani, and G. Yang, "Design of an unbalanced high power three-winding planar transformer for electric vehicle application," in *PCIM Europe 2019; International Exhibition and Conference for Power Electronics, Intelligent Motion, Renewable Energy and Energy Management*, pp. 1–8, 2019.

[8] Ziwei Ouyang, Zhe Zhang, O. C. Thomsen, and M. A. E. Andersen, "Planar-Integrated Magnetics (PIM) Module in Hybrid Bidirectional DC–DC Converter for Fuel Cell Application," *IEEE Transactions on Power Electronics*, vol. 26, pp. 3254–3264, Nov. 2011.

[9] Z. Ouyang, O. C. Thomsen, and M. A. E. Andersen, "Optimal Design and Tradeoff Analysis of Planar Transformer in High-Power DC–DC Converters," *IEEE Transactions on Industrial Electronics*, vol. 59, pp. 2800–2810, July 2012.

[10] V. Nabaei, S. A. Mousavi, K. Miralikhani, and H. Mohseni, "Balancing Current Distribution in Parallel Windings of Furnace Transformers Using the Genetic Algorithm," *IEEE Transactions on Magnetics*, vol. 46, pp. 626–629, Feb. 2010.

[11] S. Stegen and J. Lu, "Structure Comparison of High-Frequency Planar Power Integrated Magnetic Circuits," *IEEE Transactions on Magnetics*, vol. 47, pp. 4425–4428, Oct. 2011.

[12] S. Stegen and J. Lu, "Investigation of a Novel Integrated Magnetic System Using Finite Element Method in Comparison to Conventional Integrated Magnetic Devices," *IEEE Transactions on Magnetics*, vol. 48, pp. 695–698, Feb. 2012.

[13] B. Li, "High-Frequency PCB Winding Transformer With Integrated Inductors for a Bi-Directional Resonant Converter," *IEEE TRANSACTIONS ON POWER ELECTRONICS*, vol. 34, no. 7, p. 13, 2019.

[14] S. Djuric, G. Stojanovic, M. Damnjanovic, M. Radovanovic, and E. Laboure, "Design, Modeling, and Analysis of a Compact Planar Transformer," *IEEE Transactions on Magnetics*, vol. 48, pp. 4135–4138, Nov. 2012.

[15] M. Chen, M. Araghchini, K. K. Afridi, J. H. Lang, C. R. Sullivan, and D. J. Perreault, "A Systematic Approach to Modeling Impedances and Current Distribution in Planar Magnetics," *IEEE Transactions on Power Electronics*, vol. 31, pp. 560–580, Jan. 2016.

[16] R. Prieto, J. A. Oliver, J. A. Cobos, and M. Christini, "Magnetic Component Model for Planar Structures Based on Transmission Lines," *IEEE Transactions on Industrial Electronics*, vol. 57, pp. 1663–1669, May 2010.

[17] X. Margueron, A. Besri, Y. Lembeye, and J.-P. Keradec, "Current Sharing Between Parallel Turns of a Planar Transformer: Prediction and Improvement Using a Circuit Simulation Software," *IEEE Transactions on Industry Applications*, vol. 46, no. 3, pp. 1064–1071, 2010.

[18] A. Pernia, F. Nuno, and J. Lopera, "1D/2D transformer electric model for simulation in power converters," in *Proceedings of PESC '95 - Power Electronics Specialist Conference*, vol. 2, (Atlanta, GA, USA), pp. 1043–1049, IEEE, 1995.

[19] Wei Chen, Yipeng Yan, Yuequan Hu, and Qing Lu, "Model and design of PCB parallel winding for planar transformer," *IEEE Transactions on Magnetics*, vol. 39, pp. 3202–3204, Sept. 2003.

[20] P. Dowell, "Effects of eddy currents in transformer windings," *Proceedings of the Institution of Electrical Engineers*, vol. 113, no. 8, p. 1387, 1966.

[21] J.-P. Vandelac and P. D. Ziogas, "A Novel Approach for Minimizing High-Frequency Transformer Copper Losses," *IEEE Transactions on Power Electronics*, p. 12, 1988.

[22] V. Niemela, G. Skutt, A. Urling, Y.-N. Chang, T. Wilson, H. Owen, and R. Wong, "Calculating the short-circuit impedances of a multi-winding transformer from its geometry," in *20th Annual IEEE Power*

Electronics Specialists Conference, (Milwaukee, WI, USA), pp. 607–617, IEEE, 1989.

[23] Z. Ouyang, J. Zhang, and W. G. Hurley, "Calculation of Leakage Inductance for High-Frequency Transformers," *IEEE Transactions on Power Electronics*, vol. 30, pp. 5769–5775, Oct. 2015.

[24] H. A. Haus and J. R. Melcher, *Introduction to Electroquasistatics and Magnetoquasistatics*. Electromagnetic fields and energy, Englewood Cliffs, N.J: Prentice Hall, 1989.

[25] J. Scherpen, D. Jeltsema, and J. Klaassens, "Lagrangian modeling and control of switching networks with integrated coupled magnetics," in *Proceedings of the 39th IEEE Conference on Decision and Control (Cat. No.00CH37187)*, vol. 4, (Sydney, NSW, Australia), pp. 4054–4059, IEEE, 2000.

[26] R. Ortega, A. Loría, P. J. Nicklasson, and H. Sira-Ramírez, *Passivity-based Control of Euler-Lagrange Systems: Mechanical, Electrical and Electromechanical Applications, Appendix B*. Communications and Control Engineering, London: Springer London, 1998.

[27] D. C. White and H. Woodson, *Electromechanical Energy Conversion*. MIT Press, 1959.

[28] J. Meisel, *Principles of electromechanical-energy conversion*. New York: McGraw-Hill, 1966. OCLC: 567642.

[29] R. P. Feynman, R. B. Leighton, and M. L. Sands, *The Feynman lectures on physics, Volume II*. 2010. OCLC: 861525314.

[30] A. D. Snider, "A quick derivation of the Lagrange multiplier method," *International Journal of Mathematical Education in Science and Technology*, vol. 12, no. 6, p. 3, 1981.

[31] D. P. Bertsekas, *Constrained Optimization and Lagrange Multiplier Methods*. Elsevier, 1982.

[32] W. G. Hurley, "Optimizing the AC Resistance of Multilayer Transformer Windings with Arbitrary Current Waveforms," *IEEE Transactions on Power Electronics*, vol. 15, no. 2, p. 8, 2000.